

Robustness of Precast Concrete Frames: Experimental and Computational Studies

Joseph A. Main¹, Yihai Bao², H.S. Lew³, and Fahim Sadek⁴

Engineering Laboratory, National Institute of Standards and Technology
100 Bureau Drive, Mail Stop 8611, Gaithersburg, MD 20899-8611

¹Tel: (301) 975-5286; E-mail: joseph.main@nist.gov

²Tel: (301) 975-2061; E-mail: yihai.bao@nist.gov

³Tel: (301) 975-6060; E-mail: hai.lew@nist.gov

⁴Tel: (301) 975-4420; E-mail: fahim.sadek@nist.gov

ABSTRACT

This paper describes both full-scale testing and detailed finite-element modeling of a precast concrete moment-frame assembly extracted from the perimeter moment frame of a 10-story prototype building. The assembly comprises two beam spans and three columns, and the unsupported center column is subjected to monotonically increasing downward displacement to simulate a column loss scenario. Failure of the assembly was due to non-ductile fracture of the bottom anchorage bars near the welded connection to the center column. Component-level testing of the welded connection detail revealed reductions in ductility of the anchorage bar in the heat-affected zone where the bar was welded to a connecting angle. Finite element analyses revealed that large bending moments, due to eccentricities in the welded connection details, also contributed to the premature fracture of the anchorage bars in the moment-frame assembly. Finite element analyses and comparisons with experimental measurements also provide insight into the load-carrying mechanisms of the precast concrete assembly, including initial flexural action followed by arching action.

INTRODUCTION

Design of buildings with sufficient robustness to prevent disproportionate collapse under local failure scenarios is an important consideration for U.S. government and military buildings, as well as for some prominent privately owned buildings. While a large body of research has been devoted to the disproportionate collapse resistance of steel and cast-in-place concrete frame buildings (see e.g., Sadek et al. 2011), the robustness of precast concrete buildings has received comparatively little attention.

As part of a multi-year research study on mitigation of disproportionate collapse in buildings, the National Institute of Standards and Technology (NIST), in partnership with industry, has developed designs for two prototype 10-story precast concrete buildings. Two-span beam-column subassemblies from these prototype precast buildings have been tested at full scale under simulated column removal

scenarios. Similar tests have been performed previously for steel and cast-in-place concrete moment frame assemblies (Sadek et al. 2010, Lew et al. 2011).

To examine the effectiveness of seismic design and detailing on the disproportionate collapse resistance of precast concrete buildings, alternative designs were developed for Seismic Design Category B (SDC B) and SDC D. Both buildings have perimeter moment frames designed to resist lateral loads, while the interior framing is designed for gravity loads only. The building designed for SDC B incorporates ordinary moment frames (OMFs), while the building designed for SDC D incorporates special moment frames (SMFs). The perimeter moment frames consist of spandrel beams connected to columns by welded steel plates and angles. This paper presents full-scale testing and computational modeling of a beam-column subassembly extracted from the prototype SMF building. Results of full-scale testing and computational modeling of a beam-column subassembly extracted from the prototype OMF building will be reported in subsequent publications.

PROTOTYPE BUILDING DESIGN

A square plan was chosen for the prototype buildings with plan dimensions of 150 ft \times 150 ft (45.7 m \times 45.7 m). The height of the first story is 15 ft (4.6 m), and the height of each upper story is 13 ft (3.9 m). The prototype buildings were designed according to ASCE 7-05 (ASCE 2005) for Occupancy Category II. The SMF building is assumed to be located in Seattle, WA on Site Class D. Figure 1 shows the plan layout and elevation view of the SMF building.

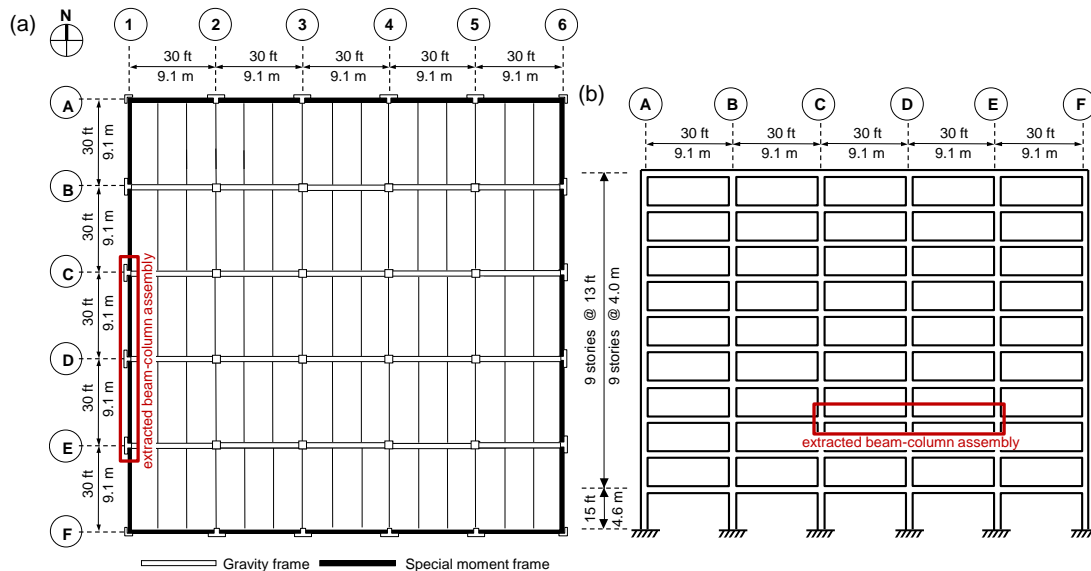


Figure 1. Prototype SMF building: (a) plan view; (b) elevation view.

The exterior framing of the prototype buildings consists of columns and spandrel beams and is designed to provide the lateral load resisting system of the building. The interior framing consists of gravity columns and simply supported Inverted-T beams. The floor system consists of Double-T members. The design of the structural members is based on the requirements of the ACI 318-05 code (ACI 2005).

The design of the beam edges is based on the PCI Design Handbook (PCI 2004). Moment transfer between an external spandrel beam and an external column is accomplished through steel link plates that are welded to steel angles embedded in the spandrel beams and to the steel plates embedded in the external columns (see Fig. 2). The axial force in the link plate is transmitted to the beam via the anchorage reinforcing bars which are welded to the inside face of the steel angle. All structural members are designed using normal weight concrete with a nominal compressive strength of 4000 psi (27.6 MPa), and reinforcing bars with a minimum specified yield strength of $f_y = 60$ ksi (414 MPa).

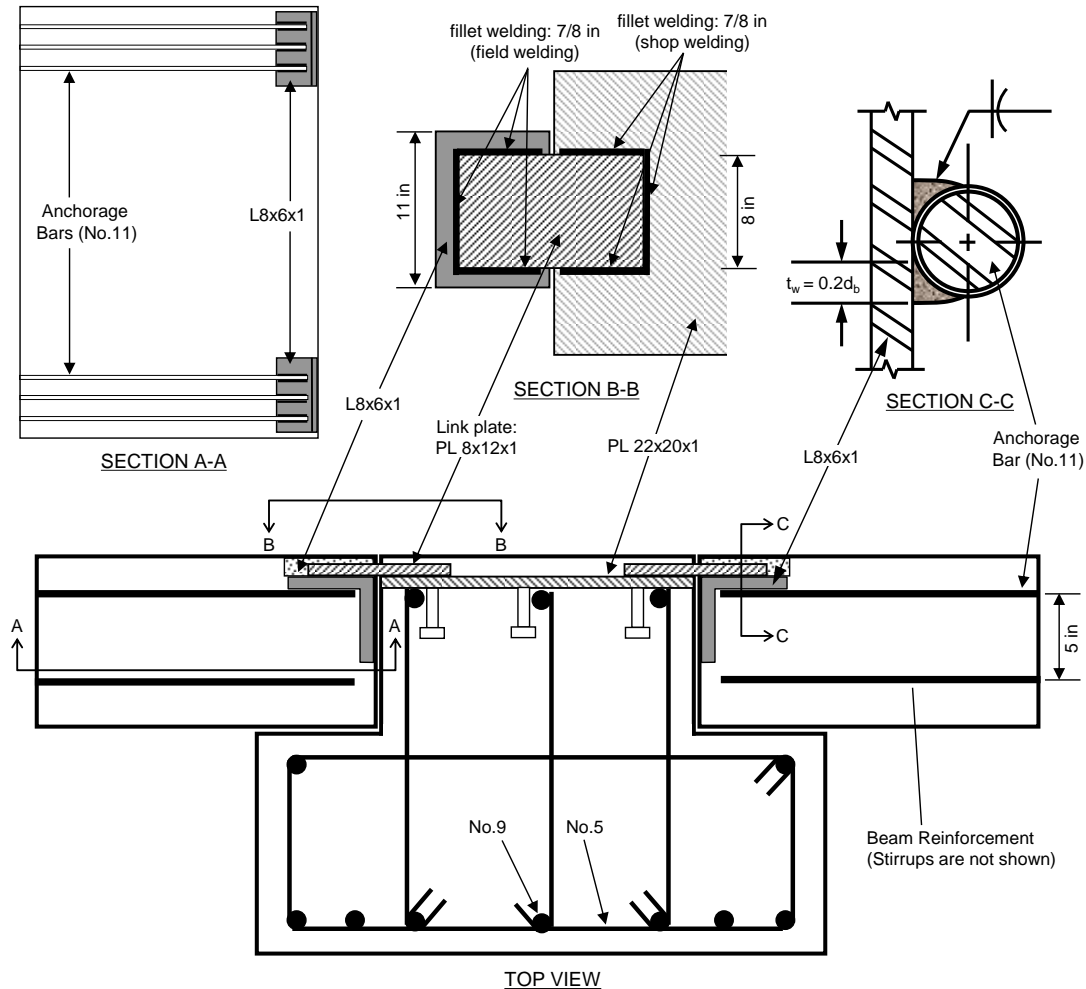


Figure 2. Beam-to-column connection details for SMF building.
(Dimensions in inches where 1 in = 25.4 mm)

TEST PROGRAM

Test specimen. The SMF specimen was a two-span beam-column assembly extracted from the third-floor framing system in the north-south direction (C1~E1) of the prototype SMF building (see Figure 1). The span length of the test specimen was reduced from 30 ft (9.14 m) to 25 ft (7.62 m) to fit within the test facility, while the

other dimensions and the connection details were unchanged from the prototype building design. Figure 3 shows member cross sections and beam-to-column connection details for the SMF specimen. All beams and columns were designed with concrete having a nominal compressive strength of 4000 psi (27.6 MPa) with ASTM A706-Grade 60 reinforcing bars with a minimum specified yield strength of $f_y = 60$ ksi (413.7 MPa).

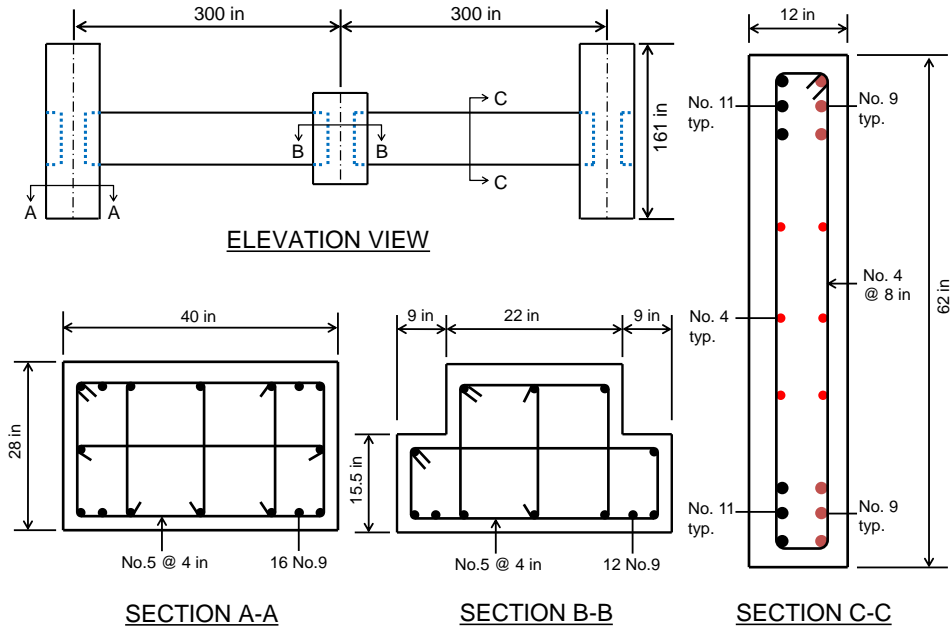


Figure 3. Member cross sections for SMF specimen. (1 in = 25.4 mm)

Test setup and instrumentation. The testing was conducted at the U.S. Army Engineer Research and Development Center (ERDC) in Vicksburg, MS. A schematic view of the test setup is shown in Figure 4. The tops of the two end columns were restrained from horizontal movement by a steel-frame lateral support. A hydraulic ram with a capacity of 600 kips (2669 kN) and a 20 in (508 mm) stroke was used to apply a vertical downward load to the center column of the test specimens. The load was applied under displacement control at a rate of 1 in/min (25 mm/min).

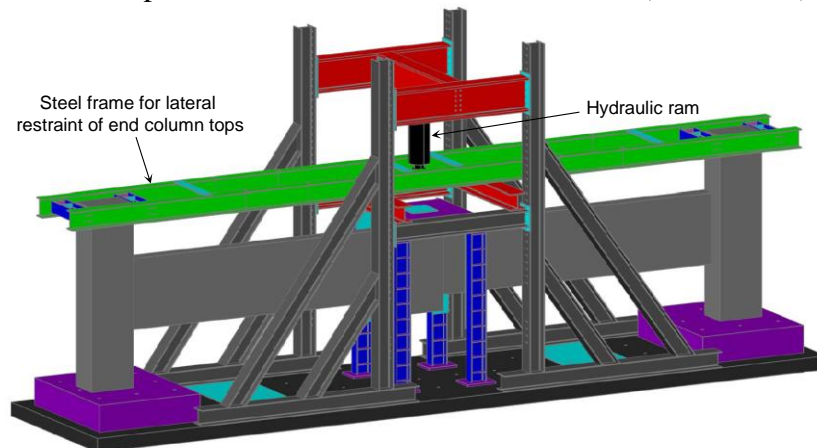


Figure 4. Schematic of test setup (Image credit: ERDC).

Instrumentation is only briefly summarized in this paper due to length limitations. Vertical displacements of the beams at various locations were measured using spring-loaded string type displacement potentiometers having a 72 in (1830 mm) range and a 0.001 in (0.025 mm) accuracy, and horizontal displacements of the end columns at the top and bottom and at beam mid-height were measured using LVDTs (linear variable differential transformers) having a 6 in (152 mm) range and a 0.005 in (0.127 mm) accuracy. To measure the rotation of the beam ends, digital inclinometers were attached to the top surface of the beams at each end. Uniaxial, electrical resistance strain gauges were attached to the surface of reinforcing bars in the beams and columns. Electrical resistance strain gauges, both uniaxial and rosette, were attached to the surface of the link plates to enable determination of horizontal, vertical, and shear strains. The estimated uncertainty in the measured data is $\pm 1\%$.

EXPERIMENTAL RESULTS

Figure 5 shows a plot of the applied vertical load versus the vertical displacement of the center column obtained from the experimental measurements. As the figure shows, the specimen was initially loaded to 89 kip (391 kN) and then unloaded, to confirm that the instrumentation, data acquisition, and loading systems were working properly. Subsequently, the specimen was loaded monotonically until the vertical displacement of the center column reached 17.7 in (450 mm), at which point large chunks of concrete were spalling from the specimen, and the test was terminated.

A significant drop in load, from 151 kip to 98 kip (672 kN to 435 kN), occurred at a vertical displacement of 2.49 in (63.3 mm), which was associated with fracture of the No. 11 anchorage bars welded to the bottom connecting angle on one side of the center column (see weld detail in Figure 2). The anchorage bars fractured at the weld location, as shown in Figure 6(a). Figures 6(b) – 6(d) show the progression of damage at the connections to the center column under increasing vertical displacement. Cracking and spalling of concrete are evident, as well as widening of the gap between the beam and column on the lower left side of the center column, where the anchorage bar fractures occurred.

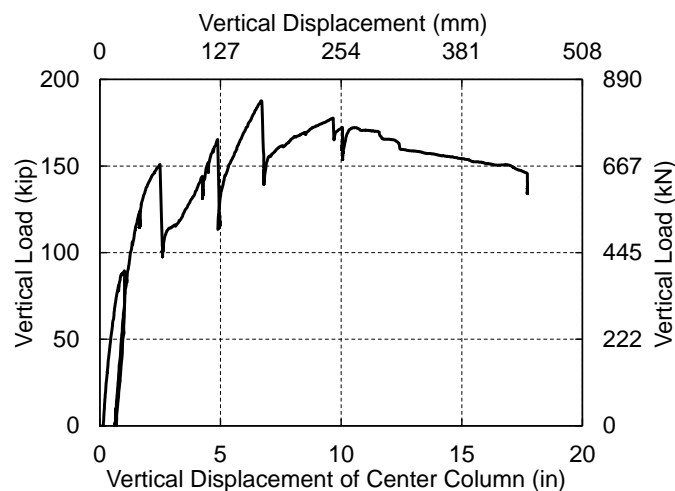


Figure 5. Vertical load versus vertical displacement of center column.

After fracture of the anchorage bars, the specimen developed additional capacity through arching action, with the top corner of each beam bearing against the center column [see Figure 6(d)], and the bottom corner of each beam bearing against the exterior columns. Significant plastic deformations of the link plates were observed, and extensive cracking and spalling of concrete occurred near the upper anchorage bars at the exterior columns. The specimen sustained an ultimate load of 188 kip (836 kN) at a center column displacement of 6.7 in (170 mm). After the column displacement exceeded 10 in (25 mm), the resistance of the specimen decreased with additional displacement of the column.

Figure 7 shows the displacement profile of the beams at different load values, obtained from the displacement potentiometer measurements along the beam spans. Some asymmetry of the displacement profile is evident, with larger displacements on the left side of the center column than on the right side. This asymmetry is a result of the anchorage bar fractures on the lower left side of the center column, which permitted in-plane rotations of the center column, as is evident in Figure 6(d). The center column displacement plotted in Figure 5 is the average of the two displacement measurements on each side of the center column.

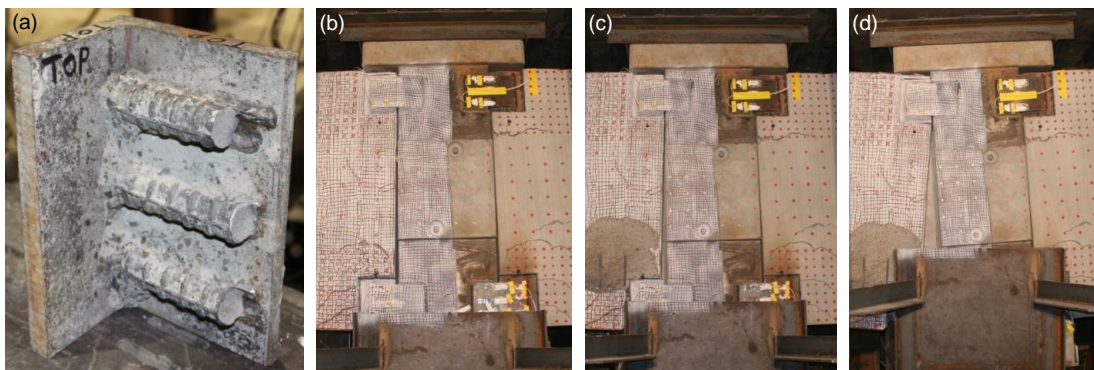


Figure 6. (a) Fractured anchorage bars; (b) – (d): Progression of damage at connections to center column.

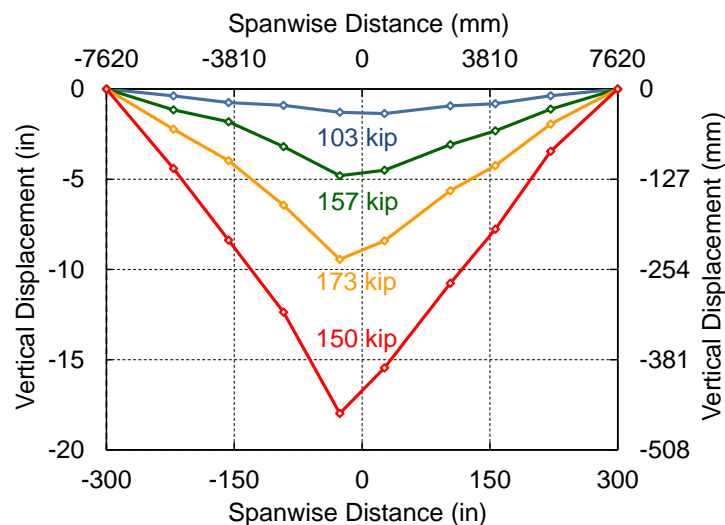


Figure 7. Vertical displacement profile of beams corresponding to indicated vertical loads (1 kip = 4.4482 kN; displacements magnified).

COMPUTATIONAL MODELING AND ANALYSIS

A detailed finite element model was developed to study the behavior and failure modes of the SMF specimen. The model consists of approximately 171,000 elements in total, including 8-node solid elements representing the concrete and the steel plates and angles and 2-node beam elements representing the reinforcing bars. The characteristic length of the solid elements ranges from 0.25 in to 2.15 in (6.35 mm to 54.6 mm). Typical beam elements range in length from 2.0 in to 5.3 in (50.8 mm to 134.6 mm), with smaller elements in locally refined regions near welded connections, as is discussed subsequently. An overview of the finite element model is shown in Figure 8 and enlarged views of local modeling details are shown in Figure 9.

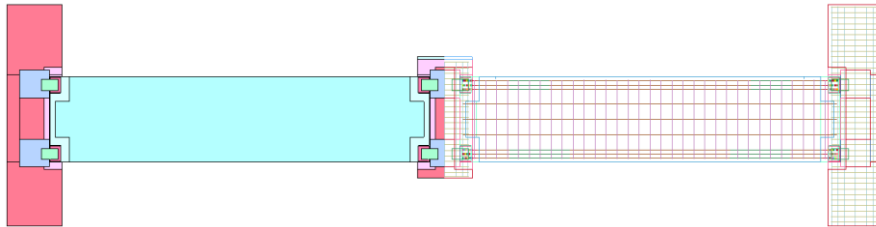


Figure 8. Overview of detailed model of SMF specimen.

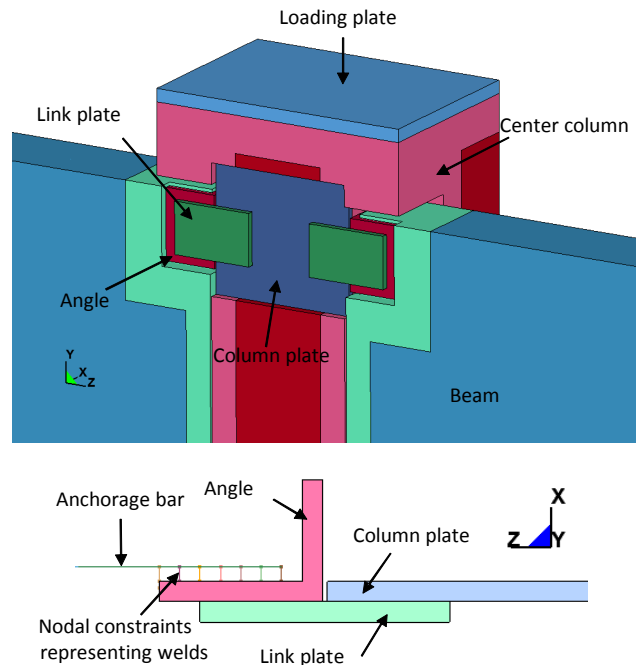


Figure 9. Enlarged views of local modeling details.

The finite element analyses presented in this study are conducted using explicit time integration in LS-DYNA (Hallquist 2007), a general-purpose finite element software package. The analyses account for both geometrical and material nonlinearities, including reinforcing bar fracture using element erosion. A contact interface is activated to prevent interpenetration and enable force transfer among the various components in the model, including the concrete beams and columns and the

steel plates and angles. In the analyses, self-weight is first applied, and then the center column is pushed down gradually under displacement control. Although explicit dynamic analysis is performed, the loads are applied slowly to ensure a quasi-static response, simulating the test conditions.

Material modeling. Concrete is modeled using a continuous surface cap model (material 159 in LS-DYNA), which captures important features of concrete behavior, including confinement effects and softening behavior both in compression and tension. A average compressive strength of 5785 psi (39.89 MPa) from a set of cylinder tests was used in the concrete model. Reinforcing bars are modeled by using an isotropic elastic-plastic model. In this model, the stress-strain relationship is defined by user input effective stress versus plastic strain curves for compression and tension separately. A plastic strain is also specified as failure strain. Once the failure strain is reached, the corresponding element is eroded, simulating fracture of the reinforcing bar. Bond slip between reinforcing bars and the surrounding concrete is assumed to have an insignificant effect on the overall response and is neglected. Steel plates are modeled using a piecewise linear plasticity model which is similar to the model used for reinforcing bars except that the same effective stress versus plastic strain curve is specified for both compression and tension. Stress-strain relationships for all reinforcing bars and steel plates are generated based on tensile test data.

Welded connection modeling. Component testing was performed to characterize the behavior of the welded connection detail shown in Figure 2, and it was found that the welding significantly reduced the ductility of the anchorage bar. Fracture of the welded anchorage bar occurred with no appreciable necking and at a significantly smaller elongation than for an isolated reinforcing bar. The stress-strain curve obtained for the welded bar was comparable to that of an isolated bar up to the ultimate stress, at which point fracture occurred without a post-ultimate softening phase. The stress-strain curve obtained for the welded bar is used for the anchorage bars near the weld, to capture the reduced ductility in the weld-affected zone.

Welds are modeled using constraints which rigidly tie nodes of different parts together. Weld failure is not considered in the model, since weld failure was determined not to be a governing failure mode. Beam elements representing reinforcing bars are modeled along the bar centerlines, and eccentricities in force transfer are captured at locations where anchorage bars are welded to the connecting angles, as shown in Figure 9. These eccentricities, caused by the offset between the centerline of each anchorage bar and the surface of the connecting angle, produce significant local bending moments in the anchorage bars that decay rapidly along the bars' length. Cross-section integration is used in the beam elements to capture the combined axial and flexural loading in the anchorage bars near the welded connections, and a refined mesh is used in this region to capture the steep gradients in bending moment.

Analysis results. Figure 10 shows a comparison of the experimental load-displacement curve for the SMF specimen (from Figure 5) with the corresponding

curve obtained from the detailed finite element model, and reasonably good agreement is observed. The finite element model indicates anchorage bar fracture occurring at a center column displacement of 2.56 in (65.0 mm), which compares well with the experimentally observed value of 2.49 in (63.3 mm). However, the load at fracture computed from the finite element model is about 23 % larger than the measured value. Figure 11(a) shows a section view through the bottom anchorage bar at the center column just prior to fracture, with contours of bending moment in the reinforcing bars indicated. Locally high values of bending moment are evident in the anchorage bar at the end of the weld to the connecting angle, where a kink in the bar is evident, associated with the formation of a plastic hinge. The locally high values of bending moment decay rapidly along the length of the bar, requiring a refined mesh to capture this effect. The interaction diagram in Figure 11(b) shows that the ultimate fracture of the anchorage bar is due to a combination of bending moment and axial force, with the bending moment exceeding the yield moment M_y and the axial force approaching the yield capacity T_y .

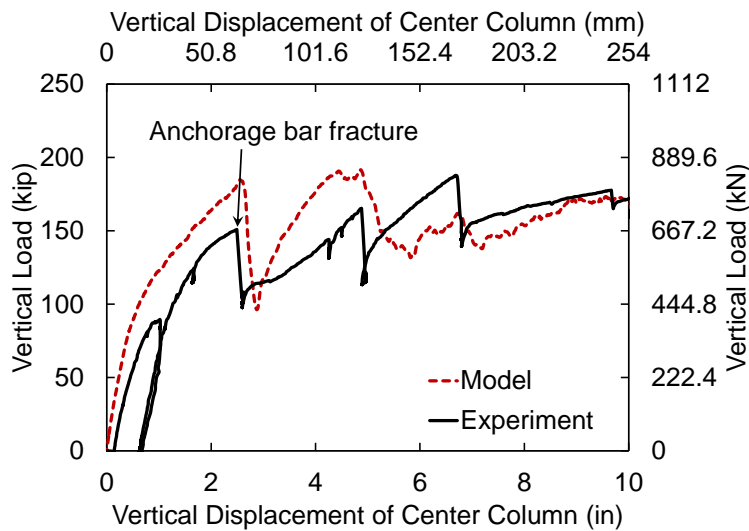


Figure 10. Comparison of experimental and computed load-displacement curves.

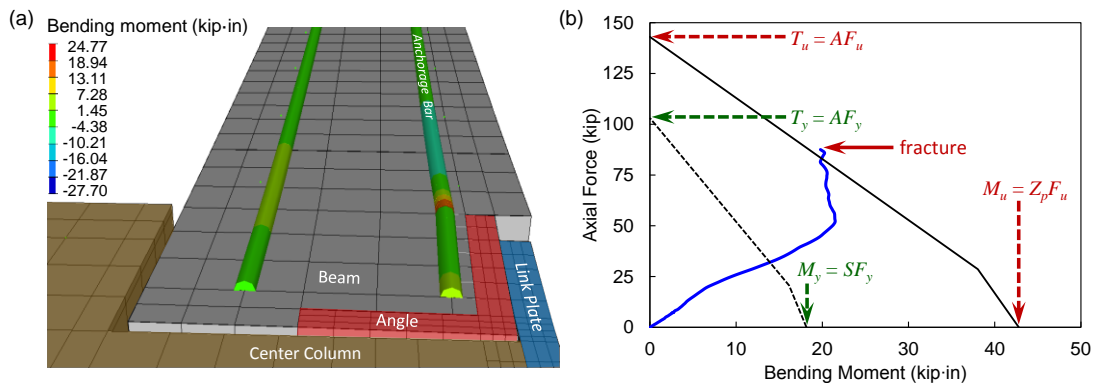


Figure 11. (a) Section view showing contours of bending moment in bottom anchorage bar at center column prior to fracture; (b) diagram showing interaction of bending moment and axial force for bottom anchorage bar. (1 kip = 4.4482 kN; 1 kip-in = 0.11298 kN·m)

After anchorage bar fracture, the model shows an increase in load associated with the development of arching action. The ultimate capacity obtained from the model is 192 kip (852 kN), which is 2 % larger than the experimentally measured value of 188 kip (836 kN). Figure 12 shows the evolution of concrete damage with increasing vertical displacement of the center column, denoted Δ . The damage index in Figure 12 varies from 0 for undamaged concrete to 1 for completely failed concrete. The pattern of concrete damage in Figure 12 is generally consistent with the pattern of cracking and spalling observed experimentally.

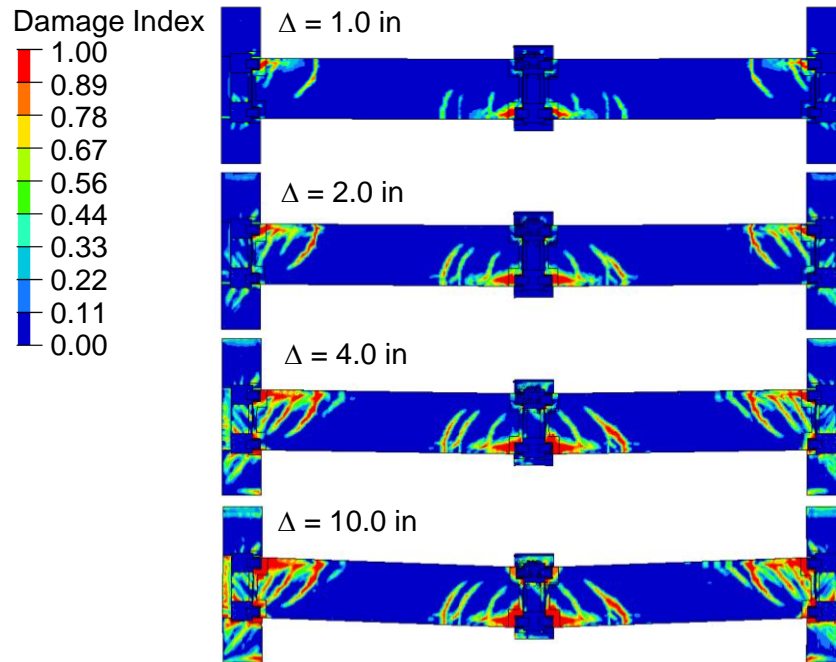


Figure 12. Evolution of concrete damage with increasing column displacement.

CONCLUSIONS

This paper described both full-scale testing and detailed finite-element modeling of a precast concrete moment-frame assembly comprising two beam spans and three columns. The center column was subjected to monotonically increasing downward displacement to simulate a column loss scenario. Initial failure of the assembly was due to non-ductile fracture of the bottom anchorage bars near the welded connection to the center column. Component-level testing of the welded connection detail revealed reductions in ductility of the anchorage bar in the heat-affected zone where the bar was welded to a connecting angle, leading to premature fracture. Finite element analyses revealed that large bending moments, due to eccentricities in the welded connection details, also contributed to the premature fracture of the anchorage bars in the moment-frame assembly. Results of the finite element model compared reasonably well with the experimental measurements and provided insights into the load-carrying mechanisms of the precast concrete assembly.

ACKNOWLEDGMENTS

The precast concrete assembly tests were performed at the US Army Engineer Research and Development Center (ERDC) in Vicksburg, MS, with significant contributions from Vincent Chiarito and Stephen Robert. The tests were supported by the National Institute of Standards and Technology, the Precast/Prestressed Concrete Institute (PCI), and the Metromont Corporation. Zhiyu Zong contributed to the finite element model development and data analysis while a Guest Researcher at NIST, and Isaiah Sampson contributed to the data analysis and plotting during a Summer Undergraduate Research Fellowship at NIST.

DISCLAIMERS

Certain commercial entities, equipment, products, or materials are identified in this document in order to describe a procedure or concept adequately. Such identification is not intended to imply recommendation, endorsement, or implication that the entities, products, materials, or equipment are necessarily the best available for the purpose. The policy of the National Institute of Standards and Technology is to use metric units in all its published materials. Because this publication is intended for the U.S. building and construction industry, which uses inch-pound units, it is more practical and less confusing to use inch-pound units in some cases, rather than metric units. However, in most cases, units are presented in both metric units and the inch-pound system.

REFERENCES

- ASCE. (2005). "Minimum design loads for buildings and other structures." *ASCE/SEI 7-05*, Reston, VA.
- American Concrete Institute (ACI). (2005). "Building Code Requirements for Structural Concrete." *ACI 318-05*, Farmington Hills, MI.
- Hallquist, J. (2007). *LS-DYNA keyword user's manual, Version 971*, Livermore Software Technology Corp., Livermore, CA.
- Lew, H.S., Bao, Y., Sadek, F., Main, J.A., Pujol, S., and Sozen, M.A. (2011). "An experimental and computational study of reinforced concrete assemblies under a column removal scenario." *NIST Technical Note 1720*, National Institute of Standards and Technology, Gaithersburg, MD.
- Precast/Prestressed Concrete Institute (PCI). (2004). *PCI Design Handbook (6th Edition)*, Chicago, IL.
- Sadek, F., Main, J.A., Lew, H.S., Robert, S.D., Chiarito, V.P., and El-Tawil, S. (2010). "An experimental and computational study of steel moment connections under a column removal scenario." *NIST Technical Note 1669*, National Institute of Standards and Technology, Gaithersburg, MD.
- Sadek, F., Main, J.A., Lew, H.S., and Bao, Y. (2011). "Testing and analysis of steel and concrete beam-column assemblies under a column removal scenario." *Journal of Structural Engineering*, 137(9), 881-892.